Partial Control of the Gulf of Mexico Dynamics by the Current Feedback to the Atmosphere

Marco Larrañaga[1] , Lionel Renault[1,2] , and Julien Jouanno[1]

(1) LEGOS, Université de Toulouse, CNES-CNRS-IRD-UPS, 14 Avenue Edouard Belin, 31400 Toulouse, France.

(2) Department of Atmospheric and Oceanic Sciences, University of California, Los Angeles, California, USA.

Corresponding author: Marco Larrañaga, marco.larranaga@legos.obs-mip.fr

Early Online Release: This preliminary version has been accepted for publication in *Journal of Physical Oceanography* cited, and has been assigned DOI 10.1175/JPO-D-21-0271.1.The final typeset copyedited article will replace the EOR at the above DOI when it is published.

ABSTRACT: The surface oceanic Currents FeedBack to the atmosphere (CFB) has been shown to correct long-lasting biases in the representation of ocean dynamics by providing an unambiguous energy sink mechanism. However its effects on the Gulf of Mexico (GoM) oceanic circulation are not known. Here, twin ocean-atmosphere eddy rich coupled simulations, with and without CFB, are performed for the period 1993-2016 over the GoM to assess to which extent CFB modulates the GoM dynamics. CFB, through the eddy killing mechanism and the associated transfer of momentum from mesoscale currents to the atmosphere, damps the mesoscale activity by roughly 20% and alters eddy statistics. We furthermore show that the Loop Current (LC) extensions can be classified into 3 categories: a retracted LC, a canonical LC, and an elongated LC. CFB, by damping the mesoscale activity, enhance the occurrence of the elongated category (by about 7%). Finally, by increasing the LC extension, CFB plays a key role in determining LC eddy separations and statistics. Taking into account CFB improves the representation of the GoM dynamics and should be taken into account in ocean models.

Accepted for publication in *Journal of Physical Oceanography*. DOI 10.1175/JPO-D-21-0271.1

1. Introduction

The Gulf of Mexico (GoM) is a semi–enclosed basin connected to the Caribbean Sea through the Yucatan Channel and to the Atlantic Ocean through the Florida Straits (Fig. 1). The more energetic feature of the GoM is the so–called Loop Current (LC), which joins the Yucatan Current and the Florida Current (Fig. 1b). On average, the LC transports about 27 Sv (1 Sv = 10^6 m^3 s^{-1}; Athié et al. 2020) while its surface velocities can be larger than 2 m s^{-1} (Coronado et al. 2007). The LC is characterized by a fluctuating northward extension (Hurlburt and Thompson 1980) that can reach lengths up to 1300 km, and extends up to 28.1°N and 85.8°W (Leben 2005). The LC sheds with periods varying between 6 and 11 months large anticyclonic eddies, generally referred to as LC eddies (Sturges and Leben 2000; Zavala-Hidalgo et al. 2006; Garcia-Jove et al. 2016). These eddies can be re-attached into the LC several times until their final separation (Leben 2005). LC eddies propagate toward the Western GoM, bringing salty water (Sosa-Gutiérrez et al. 2020; Meunier et al. 2018, 2020) and structuring the biogeochemical activity over long periods (Damien et al. 2021). Eventually, LC eddies vanish along the shelf of the Western GoM.

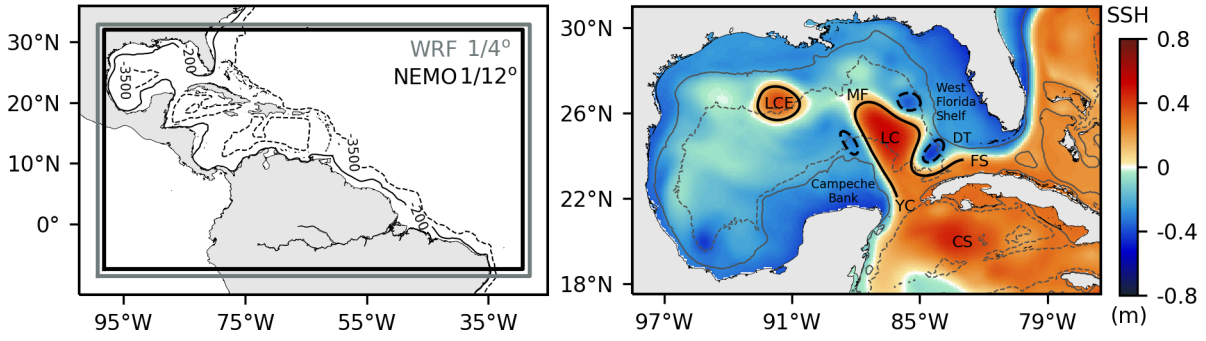

FIG. 1. Intra–Americas Sea (a) and Gulf of Mexico (b). a) The numerical domain for NEMO (WRF) is represented by the black (gray) box. The isobaths represent the 200 m (continuous lines) and 3500 m (dashed lines) depths. b) Main dynamical features of the GoM dynamics illustrated by a snapshot of the sea surface height anomaly. The continuous contours highlight the Loop Current (LC) and LC eddies. The dashed contours highlight the LC frontal eddies. YC to Yucatan Channel, FS to Florida Straits, DT to Dry Tortugas islands, MF to Mississippi Fan, and CS to Caribbean Sea. The light gray contours refer to the 200 m (continuous) and 2500 m (dashed) depths.

Several theories have been developed to explain the mechanisms that drive the LC eddy shedding. The Pichevin–Nof mechanism (Pichevin and Nof 1997) explains the eddy detachment by a westward

Accepted for publication in *Journal of Physical Oceanography*. DOI 10.1175/JPO-D-21-0271.1

propagation of an eddy (as a Rossby wave) that exceeds the growth of the LC by using a reduced–gravity model. Chang and Oey (2013) shows that the LC variability and the associated eddy shedding could be modulated by the biannually varying trade winds in the Caribbean Sea, which partially control transport in the Yucatan Channel. Candela et al. (2002), Sheinbaum (2002) and Sheinbaum et al. (2016) suggest that mesoscale eddies from the Caribbean Sea interact with the LC, triggering LC eddy detachments. Finally, several studies highlight the interactions between the LC and cyclonic eddies that travel around its periphery (segmented contours in Fig. 1b; Fratantoni et al. 1998; Le Hénaff et al. 2012; Zavala-Hidalgo et al. 2006; Jouanno et al. 2016; Hiron et al. 2020). These LC frontal eddies are principally generated at the east of the Campeche Bank and grow while traveling along with the LC (Jouanno et al. 2016; Hiron et al. 2020). Larger stationary cyclonic eddies (diameter of ∼100–200 km), the so-called Tortugas eddies, are also found in the southeastern region of the LC (Fig. 1b). On the one hand, these cyclonic eddies (either LC frontal eddies or Tortugas eddies) have been suggested to play a key role in determining the LC eddies shedding (Vukovich and Maul 1985; Schmitz 2005; Fratantoni et al. 1998; Zavala-Hidalgo et al. 2003). On the other hand, they can also block the LC penetration into the GoM, which in turn increases the period between eddies shedding (Zavala-Hidalgo et al. 2003, 2006).

Understanding and forecasting the GoM dynamics is of uttermost importance to face up increasing environmental issues such as oil spills (Kostka et al. 2011; White et al. 2012; Michel et al. 2013), plastics (Phillips and Bonner 2015), or the massive arrival of Sargassum in the region (Gower et al. 2006; Gower and King 2011; Wang and Hu 2017; Cuevas et al. 2018). Numerical models can simulate the main characteristics of the GoM dynamics, but most models are characterized by persistent biases in *e.g.,* the LC penetration into the GoM and the LC eddy detachments, which makes the representation of the GoM dynamics and its forecast challenging for modelers (Le Hénaff et al. 2012; Garcia-Jove et al. 2016; Putrasahan et al. 2017).

One aspect of the GoM that has been little studied concerns the role of mesoscale air–sea interactions on the determination of its dynamics. In the last decades, and principally over other regions, two main air–sea interactions have been assessed: the thermal feedback, *i.e.,* the influence of Sea Surface Temperature (SST) on the atmosphere, and the Current Feedback (CFB), *i.e.,* the influence of sea surface currents on the atmosphere. Small et al. (2008) provides a review of the different processes involved in the thermal feedback. Ma et al. (2016) and Seo et al. (2017)

Accepted for publication in *Journal of Physical Oceanography*. DOI 10.1175/JPO-D-21-0271.1

suggest that the mesoscale thermal feedback, by causing turbulent heat fluxes anomalies, could modulate Western Boundary Currents. Recently Putrasahan et al. (2017) highlight the role of the mesoscale thermal feedback in determining surface turbulent heat fluxes in the GoM. The CFB has a "bottom-up" effect on on the wind by directly modifying the surface stress Bye 1985: a negative current anomaly induces a positive stress anomaly, which in turn causes a negative wind anomaly (Renault et al. 2016b)). CFB has been shown to largely modulate the ocean dynamics, partly correcting long–lasting biases in ocean models. At the large scale, CFB reduces both the wind stress and the transfer of energy from the atmosphere to the ocean when surface currents and winds have the same directions and increase the wind stress and the transfer of energy from the ocean to the atmosphere when surface currents and winds are in opposite directions (Fig. 5 and 6 in Renault et al. 2016a). As a result, it slows down the mean circulation regardless of the wind and currents direction (Pacanowski 1987; Luo et al. 2005). At the mesoscale, by modulating the surface stress, CFB induces the so-called eddy killing mechanism: a sink of momentum from the ocean to the atmosphere that damps the mesoscale activity by roughly 30% (Renault et al. 2016b,a; Seo et al. 2016; Renault et al. 2017b; Seo et al. 2017; Oerder et al. 2018; Jullien et al. 2020). Additionally, Renault et al. (2019b) demonstrate that the reduction of the mesoscale activity by CFB weakens the eddy–mean flow interactions (the inverse cascade of energy), stabilizing *e.g.,* the western boundary currents and improving their representation in numerical models. As the GoM is the place of very intense mesoscale dynamics, mesoscale air–sea interactions should play an key role in determining its dynamical equilibrium.

This study aims at examining and quantifying the extent to which CFB can control the dynamics of the GoM, with a focus on the LC dynamics and eddy shedding process. To that end, twin ocean–atmosphere coupled simulations for the GoM are carried out and analyzed over a period of 24-year. The study is organized as follows: the models, data and methodology are described in Section 2. Section 3 assesses the extent to which CFB modulates the kinetic energy (KE) and the main energy conversion terms. In Section 4 the impact of CFB on the LC variability is assessed, and Section 5 illustrates the sensitivity of LC eddies to CFB in terms on their shedding statistics and properties. Finally, the results are discussed in Section 6.

Accepted for publication in *Journal of Physical Oceanography*. DOI 10.1175/JPO-D-21-0271.1

2. Model configuration and methodology

a. Oceanic model

The oceanic simulations were performed with the Nucleus for European Modeling of the Ocean (NEMO 4.0; Madec and Team 2016). NEMO solves the three-dimensional primitive equations on an Arakawa C-grid, assuming hydrostatic equilibrium and Boussinesq approximation. The regional grid covers the Intra–Americas Sea (IAS) region extending from 7.4°S to 31.9°N and from 98.2°W to 29.3°W with a spatial resolution of 1/12° (~8 km). It covers the Gulf of Mexico, the Caribbean Sea, and the north Brazilian region (Fig. 1). The grid is composed of 75 fixed vertical levels, with 8 levels in the upper 10 m depth and 38 levels between 10 and 1000 m depth. The model time step is 400 s. Advection of tracers is performed with flux corrected transport scheme (Zalesak 1979). Horizontal diffusion of tracers and momentum are parameterized with a bi-Laplacian operator. The vertical turbulent mixing is computed using the Generic Length Scale scheme (GLS, Umlauf and Burchard 2003), with a k–ϵ turbulent closure model (Reffray et al. 2015; Rodi 1979). At the lateral boundaries, daily averages of temperature, salinity, sea surface elevation, and horizontal velocity are prescribed from the Global Mercator reanalysis (GLORYS2V4; Lellouche et al. 2018). The initial condition is obtained from a previous 3–year simulation initialized with GLORYS2V4 and forced at the surface with the Drakkar Forcing Set (DFS5.2; Dussin et al. 2016), from year 1990 to 1993.

b. Atmospheric model

The Weather Research and Forecast (WRF) Model (version 4.1; Skamarock et al. 2019) is implemented in a one–grid configuration with a spatial resolution of 1/4° (25 km), and 40 terrain–following vertical levels with a surface and upper stretch factors of 1.3 and 1.1, respectively. The model time step is 75 s. ERA–Interim data is used to initialize the model and to force it at the open boundary conditions. The domain is slightly larger than the NEMO domain to avoid the effect of the WRF sponge (4 points; Renault et al. 2019b). The WRF model allows the user to employ a wide range of parameterization. Following Gévaudan et al. (2021), who performed NEMO–WRF simulations of the Tropical Atlantic at similar resolution, this implementation includes the WRF–single–moment–microphysics class 6 scheme (WSM6, Hong and Lim 2006), the rapid radiative transfer model for the longwave flux (RRTM, Mlawer et al. 1997), the RRTMG shortwave flux

Accepted for publication in *Journal of Physical Oceanography*. DOI 10.1175/JPO-D-21-0271.1

scheme (Iacono et al. 2008), and the Yonsei University (YSU) scheme to solve the planetary boundary layer physics (Hong et al. 2006; Hong 2010), the Noah land–surface model and the Monin-Obukhov similarity scheme (Chen and Dudhia 2001). Cumulus are parameterized by the multi–scale Kain–Fritsch scheme (MSKF, Zheng et al. 2016).

c. Coupling procedure and experiments

The Ocean Atmosphere Sea Ice Sol (OASIS3-MCT, Valcke 2013) software is used to exchange hourly averaged data between the numerical models NEMO and WRF. Two experiments are carried out over the period 1993–2016 (24 years): NOCF (No Current Feedback) and CF (with Current Feedback). In both experiments, WRF forces NEMO with hourly momentum, heat and freshwater fluxes, while NEMO sends SST to WRF. The difference between the two experiments lies in the way these fluxes are estimated. In the NOCF experiment, the surface stress (τ) is computed by WRF as a function of the 10 m absolute wind ($\mathbf{U}_a$):

$$\boldsymbol{\tau} = \rho_a C_{\mathrm{D}} |\mathbf{U_a}| \mathbf{U_a}, \tag{1}$$

where ρ_a is the air density and C_{D} the drag coefficient.

In CF, NEMO also gives hourly averages of surface currents (U_o) to WRF, and the surface stress is estimated as a function of the relative wind (U_r):

$$\mathbf{U_r} = \mathbf{U}_a - \mathbf{U_o}. \tag{2}$$

Note that because of the implicit treatment of the bottom boundary condition in most atmospheric models (including WRF), the use of relative winds does not only involve the modification of the bulk formulae but also a modification of the tridiagonal problem associated with the discretization of the vertical turbulent viscosity. If not done properly, the CFB effect on the oceanic circulation can be largely underestimated (Lemarié et al. 2015; Renault et al. 2019a). Note that neither NEMO nor WRF include data assimilation.

Accepted for publication in *Journal of Physical Oceanography*. DOI 10.1175/JPO-D-21-0271.1

d. Energy budget

Following Marchesiello et al. (2003), a simplified energy budget is estimated focusing on the following relevant energy sources and eddy–mean conversion terms:

$$F_{\mathrm{m}}K_{\mathrm{m_g}} = \frac{1}{\rho_0}\left(\overline{u_{\mathrm{g}}}\,\overline{\tau_{\mathrm{x}}} + \overline{v_{\mathrm{g}}}\,\overline{\tau_{\mathrm{y}}}\right), \tag{3}$$

$$F_{\mathrm{e}}K_{\mathrm{e_g}} = \frac{1}{\rho_0}\left(\overline{u'_{\mathrm{g}}\tau'_{\mathrm{x}}} + \overline{v'_{\mathrm{g}}\tau'_{\mathrm{y}}}\right), \tag{4}$$

$$K_{\mathrm{m}}K_{\mathrm{e}} = -\int_z^0 \left(\overline{u'u'}\frac{\partial\overline{u}}{\partial x} + \overline{u'v'}\frac{\partial\overline{u}}{\partial y} + \overline{u'w'}\frac{\partial\overline{u}}{\partial z} + \overline{v'u'}\frac{\partial\overline{v}}{\partial x} + \overline{v'v'}\frac{\partial\overline{v}}{\partial y} + \overline{v'w'}\frac{\partial\overline{v}}{\partial z}\right) dz, \tag{5}$$

$$P_{\mathrm{e}}K_{\mathrm{e}} = \int_z^0 -\frac{g}{\rho_0}\overline{\rho'w'}\,dz, \tag{6}$$

where g is the gravitational acceleration and ρ and ρ_0 are the potential density and density reference (1026 kg/m^{-3}). u_{g} and v_{g} are the meridional and zonal geostrophic velocities at the surface, u, v and w correspond to the zonal, meridional and vertical velocities, and τ_{x} and τ_{y} the zonal and meridional wind stress. All quantities are decomposed into the long-term mean estimated over the 1993–2016 period and indicated with an overbar (-). It is worth mentioning that the anomalies are mainly related to mesoscale processes as the oceanic model does not resolve submesoscale eddies and also because the region exhibits a weak seasonal variability (not shown). Note that this assumption is valid for the open ocean but not for the continental shelf, where current anomalies are likely driven by coastal trapped waves and seasonal circulation. However, as the main object of our study is the LC and the associate eddy shedding, this assumption is wholly acceptable. Their deviations from this long–term mean are referred to using primes ($'$). $F_{\mathrm{m}}K_{\mathrm{m_g}}$ correspond to the transfer of energy between mean ocean currents and the atmosphere, $F_{\mathrm{e}}K_{\mathrm{e_g}}$ to the transfer of energy between the ocean and the atmosphere at the mesoscale, $K_{\mathrm{m}}K_{\mathrm{e}}$ to the barotropic conversion from mean kinetic energy (MKE) to mesoscale activity, and $P_{\mathrm{e}}K_{\mathrm{e}}$ to the baroclinic conversion from eddy potential energy to mesoscale activity.

e. Position of the LC and metrics

Following Leben (2005), a Sea Surface Height Anomaly (SSHa) is first estimated by removing from the SSH its long–term temporal mean and its spatial average over the GoM. The daily LC

Accepted for publication in *Journal of Physical Oceanography*. DOI 10.1175/JPO-D-21-0271.1

position is then inferred from the 17 cm SSHa contour, starting from the Yucatan Channel and ending at the Florida Straits. Once the LC is detected, the maximum North latitude, minimum East longitude, and LC length are used to infer the LC penetration into the GoM. In addition, as a proxy of the energy stored by the LC, the surface KE is integrated within the 17 cm SSHa contour.

f. LC eddies detection

The eddy tracking detection method developed by Chaigneau et al. (2009) and implemented over the GoM by Sosa-Gutiérrez et al. (2020) is used to detect and track LC eddies. This approach consists of detecting local maxima in daily Sea Level Anomaly (SLA) maps that are associated with the center of anticyclonic eddies. The detection method identifies the outermost closed contour of SLA for each eddy center and associates it with the eddy edge. The eddies are tracked by an algorithm developed by Pegliasco et al. (2015), which computes eddy trajectories by the intersection of eddies along with daily maps. In this study, LC eddies are defined as eddies separated from the LC with a lifetime larger than 200 days (Sosa-Gutiérrez et al. 2020; Chelton et al. 2011).

3. Modulation of the Kinetic energy and Energy Conversion by CFB

a. Mean and Eddy Kinetic Energy

As a proxy of the mean surface circulation, the geostrophic surface Mean Kinetic Energy (MKE, Fig. 2a) is estimated using the long-term mean geostrophic currents from the 1/4°AVISO daily fields product distributed by the Copernicus Marine and Environment Monitoring Service (CMEMS; https://www.copernicus.eu). Consistent with Leben (2005), the GoM mean circulation is marked by the presence of the LC that extends up to 26.3°N and 87.8°W, with northwestward and southwestward flows well defined reaching up to 0.5 m^2s^{-2}. The surface geostrophic eddy kinetic energy (EKE) is furthermore estimated over the 1993–2016 period from AVISO (Fig. 2d). The EKE is greatest over the LC, in the northern and western regions of the LC, and west of the Florida Shelf with values of about 0.15 m^2s^{-2}. It reaches its maximum values (0.25 m^2s^{-2}) near the Dry Tortugas Islands, where the quasi-stationary Tortugas eddies are generated (Fratantoni et al. 1998). From the LC region to the west of the GoM, the EKE is also characterized by a zonal band of relatively large energy values (0.06 m^2s^{-2}), which is mainly related to the westward propagation of LC eddies.

Accepted for publication in *Journal of Physical Oceanography*. DOI 10.1175/JPO-D-21-0271.1

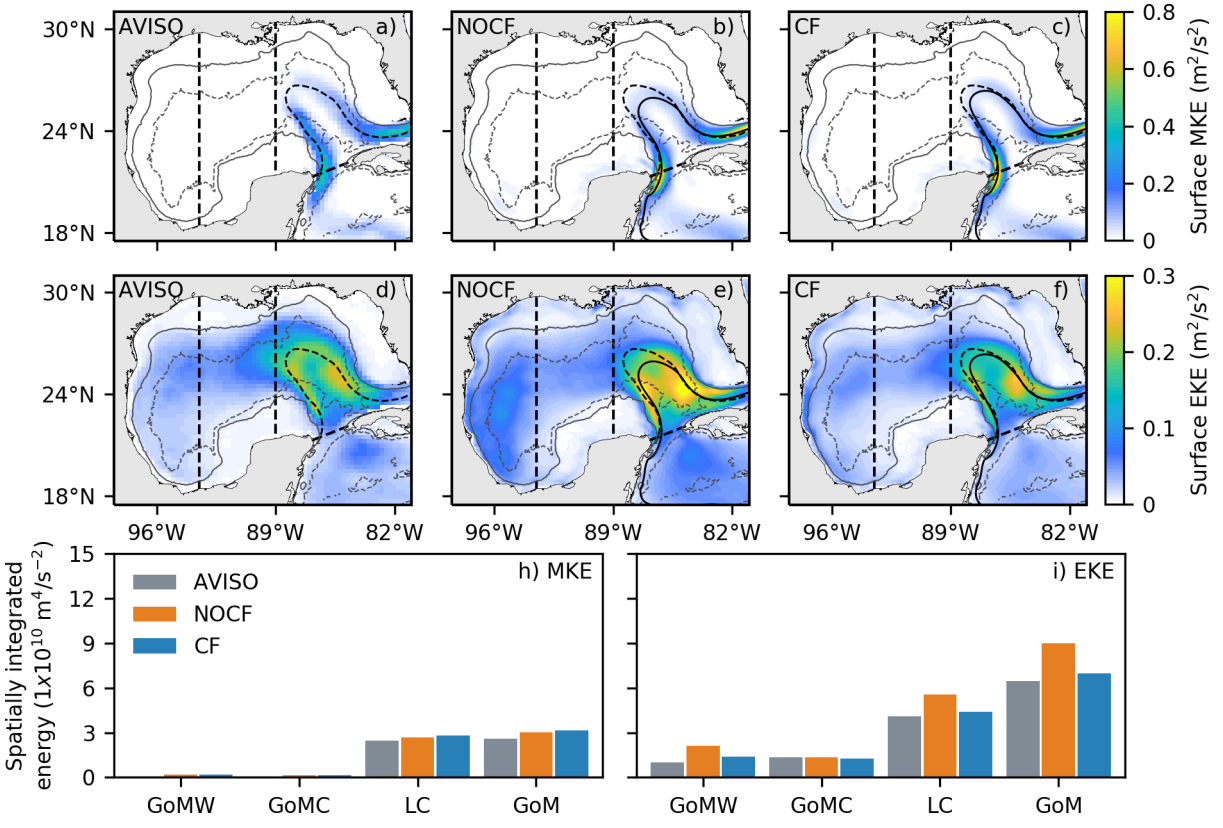

FIG. 2. Surface mean kinetic energy (first row) and eddy kinetic energy (second row) climatologies (1993–2016) from AVISO (first column), NOCF (second column) and CF (second column). The 17 cm contours of the climatological sea surface height anomaly of AVISO and the numerical experiments are represented by the thin segmented line and the continuous line, respectively. The thick segmented lines delimit the LC (east), center (GoMC) and west (GoMW) regions. GoM makes reference to the whole Gulf of Mexico. The light gray contours refers to the 200 (continuous) and 2500 m (segmented) depths. Spatially integrated values over regions are shown in the last row.

The MKE and EKE are furthermore estimated from NOCF and CF (Fig. 2). Both experiments have a realistic representation of the mean features of the GoM surface circulation with respect to AVISO. Consistent with previous studies in other regions, CFB improves the realism of the simulations by reducing biases with respect to AVISO, *e.g.,* increasing the mean LC penetration into the GoM. CFB has two main effects on the GoM circulation. On the one hand, CFB causes a damping of the mesoscale activity (Figs. 2e,f). From NOCF to CFB, on average, the EKE in the GoM region is reduced by 22% (Fig. 2i) while its spatial pattern is improved with respect to AVISO (Figs. 2d-f). On the other hand, even if at the large-scale CFB slows down the mean

Accepted for publication in *Journal of Physical Oceanography*. DOI 10.1175/JPO-D-21-0271.1

circulation (Luo et al. 2005; Renault et al. 2016a, 2017b), CFB stabilizes and narrows mean currents in regions with a large mesoscale activity, such as intensified boundary currents (Renault et al. 2019b, 2021a). In a similar way, the mean LC have stronger and narrower currents when CFB is considered. Indeed, as shpwn in (Fig. 3a), the current is concentrated towards the coast near Campeche Bank, and outward the coast near Tortugas Islands. This is likely explained by a weaker eddy–mean flow interaction in CF with respect to NOCF, and occur where CFB damps a larger amount of EKE (Fig. 3b). As a results, from NOCF to CF, the slow-down of the large-scale circulation is counter-balanced by an intensified and more stable LC, resulting in a similar MKE integrated over the LC region (Fig. 2h-i). Interestingly, the patch of larger EKE values in CF with respect NOCF (northwestern region of the LC; Fig. 3b) results from a change of path of the LC extension and of the LC eddies detachment statistics and trajectories (see sections 4 and 5).

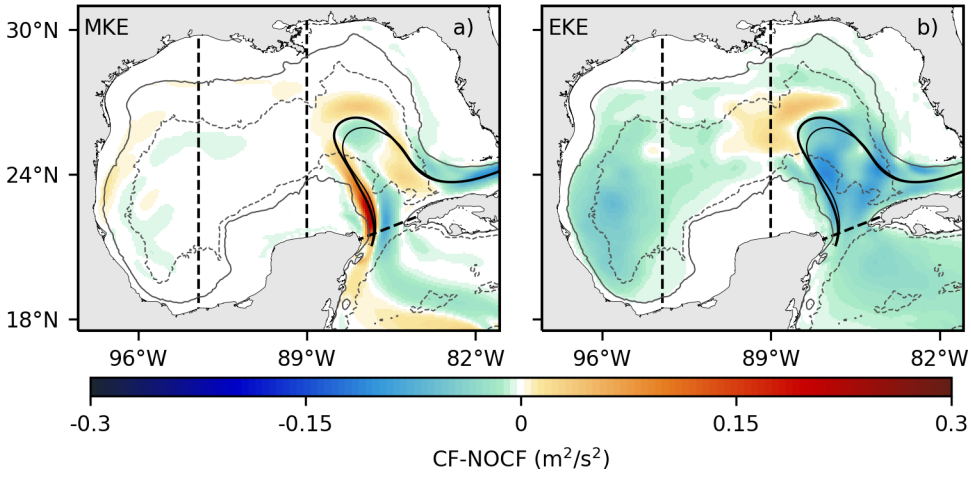

FIG. 3. Difference between CF (a) and NOCF (b) EKE climatologies (1993–2016). The 17 cm contours of the climatological sea surface height anomaly of NOCF and CF experiments are represented by the black thin line and the black thick line, respectively. The thick segmented lines delimit the LC (east), center (GoMC) and west (GoMW) regions. GoM makes reference to the whole Gulf of Mexico. The light gray contours refers to the 200 (continuous) and 2500 m (segmented) depths.

CF still has some discrepancies with AVISO. The EKE over the LC is overestimated by 7% (*vs.* 28% in NOCF) and the MKE by 40% over the Yucatan Channel. While no doubt some of these are due to model biases, there are important sampling differences between AVISO and model outputs. Indeed, AVISO sea level anomaly can only resolve eddies with a radius larger than about 40 km and a lifetime longer than one week (Chelton et al. 2011; Amores et al. 2018; Archer et al.

Accepted for publication in *Journal of Physical Oceanography*. DOI 10.1175/JPO-D-21-0271.1

2020). In particular, the AVISO data has spatial and temporal resolutions issues and only detect the signature of the larger mesoscale eddies (Chelton et al. 2011; Amores et al. 2018; Archer et al. 2020). Additionally, observations from a mooring array over the GoM (Athié et al. 2015) reveal that AVISO underestimates the western current at the Yucatan Channel by about ~38% (Fig. 4). This is confirmed by comparing surface current speeds from the simulations to those inferred from a mooring array (Athié et al. 2015) positioned across the Yucatan channel during the period 1992–2001 and 2010–2011 (Figure 4). Consistent with the previous results, the mean surface currents in CF are in better agreement with the observations than those in NOCF in terms of velocity and spatial pattern (Fig. 4).

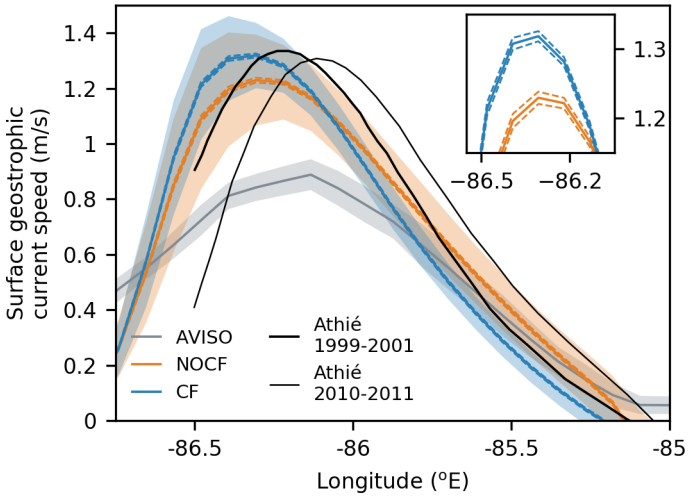

FIG. 4. Mean (solid lines) and standard deviation (shading area) of geostrophic currents along the Yucatan Channel. Segmented lines in NOCF and CF are associated to an error estimation of the mean current obtained by using a bootstrap method over 50,000 random samples. To more easily appreciate the bootstrap error bars, a zoom of the region with stronger currents in the numerical simulations is included at the upper right corner of the figure.

Noteworthy, the Yucatan Chanel current is weaker (0.1 m s^{-1}) and more spatially spread in NOCF with respect to that in CF and in the observations (Table 1), in line with the fact that CFB weakens the eddy–mean flow interactions in regions with a large mesoscale activity (Renault et al. 2019b). As a remaining bias with respect to the observations, the maximum current speed in both NOCF and CF is shifted westward (~11 km) from the maximum registered by the moorings during 1999–2001 period, and 40 km from the one registered during 2010–2011 period. However,

Accepted for publication in *Journal of Physical Oceanography*. DOI 10.1175/JPO-D-21-0271.1

TABLE 1. Statistics of Yucatan Channel current. The current width is computed as the distance between locations with velocities larger than 0.6 ms^{-1} and the current speed rate of change from the maximum speed to the eastern region of the Yucatan Channel.

	Maximum speed (ms^{-1})	Current width (km)	Current speed rate of change along the channel (ms^{-1}/km)
Athié 1999–2001	1.33	–	-0.014
Athié 2010–2011	1.31	81.00	-0.014
CF	1.32	81.00	-0.014
NOCF	1.23	90.00	-0.010
AVISO	0.89	81.00	-0.008

extensive time series are needed to better quantify the spatial variability of the Yucatan Channel current and to properly validate long–term numerical simulations.

b. Energy conversion

In order to explain the reduction of EKE from NOCF to CF, energy transfers associated with barotropic and baroclinic instabilities (K_mK_e and P_mK_e), and the mean and eddy geostrophic wind work ($F_mK_{e_g}$ and $F_eK_{e_g}$) are shown in Figs. 5 and 6. In NOCF, both K_mK_e and P_mK_e contribute to the EKE generation over the LC, with K_mK_e having the larger contribution (about 6×10^6 m^5s^{-3}; Fig. 5c). The production of EKE is primarily concentrated within the area delimited by the mean LC position inferred from the 17 cm SSHa contour in Fig. 5a,d. Besides, a large production of EKE by barotropic and baroclinic instabilities is found at the east of the Campeche Bank, the northwestern and northeastern regions of the LC, and for the area near Dry Tortugas islands. These regions are characterized by the presence and intensification of cyclonic eddies (Fratantoni et al. 1998; Zavala-Hidalgo et al. 2003; Oey 2008; Jouanno et al. 2016; Hiron et al. 2020). From NOCF to CF, both K_mK_e and P_eK_e are reduced over the mean LC position (Fig. 5). Over the LC region, K_mK_e is reduced by 14%, which is mostly compensated by a P_eK_e increase (11%).

Accepted for publication in *Journal of Physical Oceanography*. DOI 10.1175/JPO-D-21-0271.1

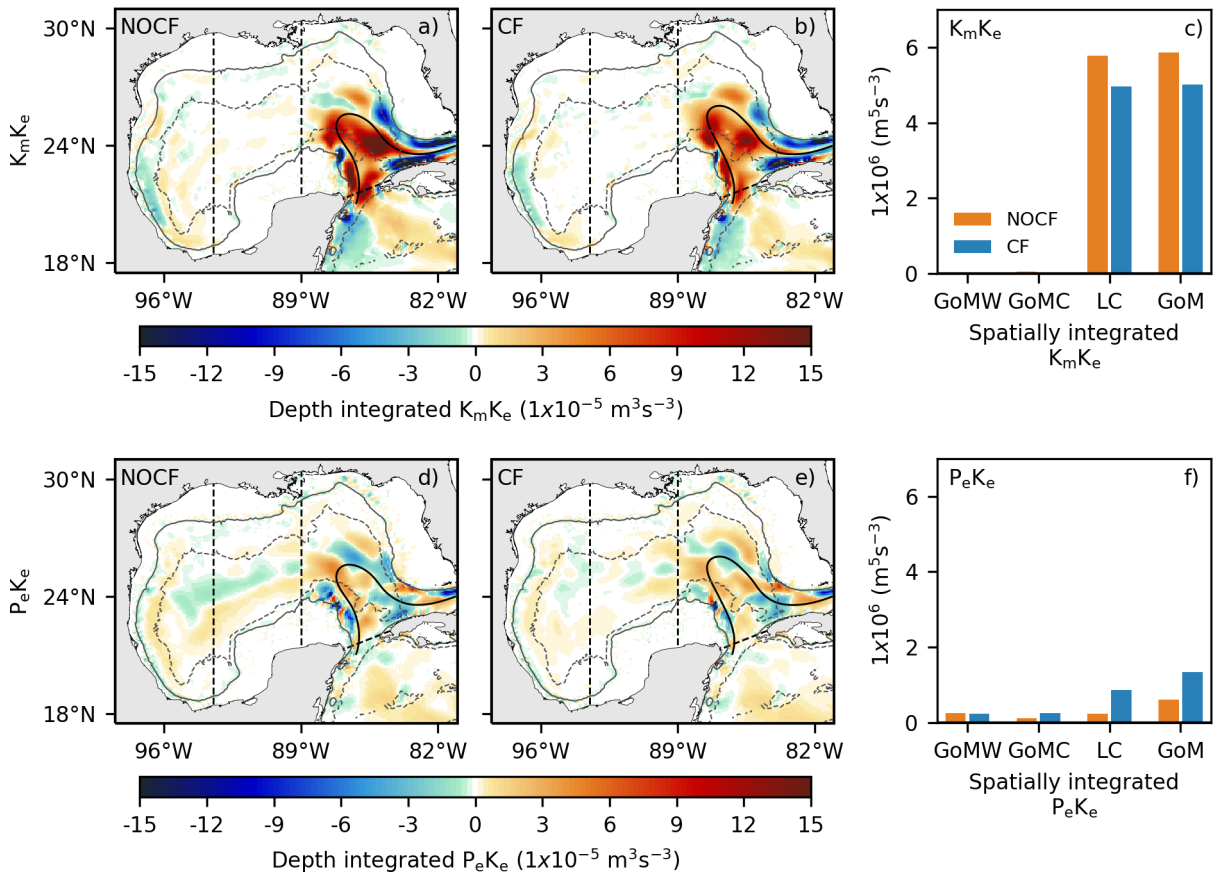

FIG. 5. Barotropic (top) and baroclinic (bottom) instabilities maps and spatially integrated values over regions (right) for the NOCF and CF experiments for the period 1993–2016. The segmented lines delimit the LC (east), center (GoMC) and west (GoMW) regions. GoM makes reference to the whole Gulf of Mexico. The light gray contours refers to the 200 (continuous) and 2500 m (segmented) depths.

Figure 6 shows the geostrophic wind work decomposed into its mean ($F_{\mathrm{m}}K_{m_g}$) and eddy ($F_{\mathrm{e}}K_{\mathrm{e_g}}$) components for NOCF and CF (See Sec. 2.d). $F_{\mathrm{e}}K_{\mathrm{e}}$ has positive values on the shelf in both NOCF and CF, which are related to wind-driven current and the resulting geostrophic current anomaly that partially flows in the same direction than the wind (Renault et al. 2016b,a). To better quantify the transfer of energy induced by CFB in the open ocean, the geostrophic eddy wind work ($F_{\mathrm{e}}K_{\mathrm{e_g}}$) is spatially integrated over regions deeper than 200 m (Figs. 6cf). In NOCF, $F_{\mathrm{e}}K_{\mathrm{e_g}}$ is characterized by alternating positive/negative values (Fig. 6a) and a weak positive average over the GoM (Fig. 6c). In contrast, $F_{\mathrm{e}}K_{\mathrm{e_g}}$ in CF is mostly negative over the entire GoM and in particular near Dry Tortugas Islands (up to -8×10^{-6} m^3s^{-3}). This reveals a sink of energy from mesoscale eddies to

Accepted for publication in *Journal of Physical Oceanography*. DOI 10.1175/JPO-D-21-0271.1

the atmosphere that causes the eddy killing mechanism and the EKE damping from NOCF to CF (Fig. 6c). Renault et al. (2016a, 2017b) report similar values for the GoM, although higher ones (about -1.5×10^{-5} m^3s^{-3}) are found over regions where the EKE and the wind are larger, such as the Gulf Stream and the Agulhas Current retroflection.

Accepted for publication in *Journal of Physical Oceanography*. DOI 10.1175/JPO-D-21-0271.1

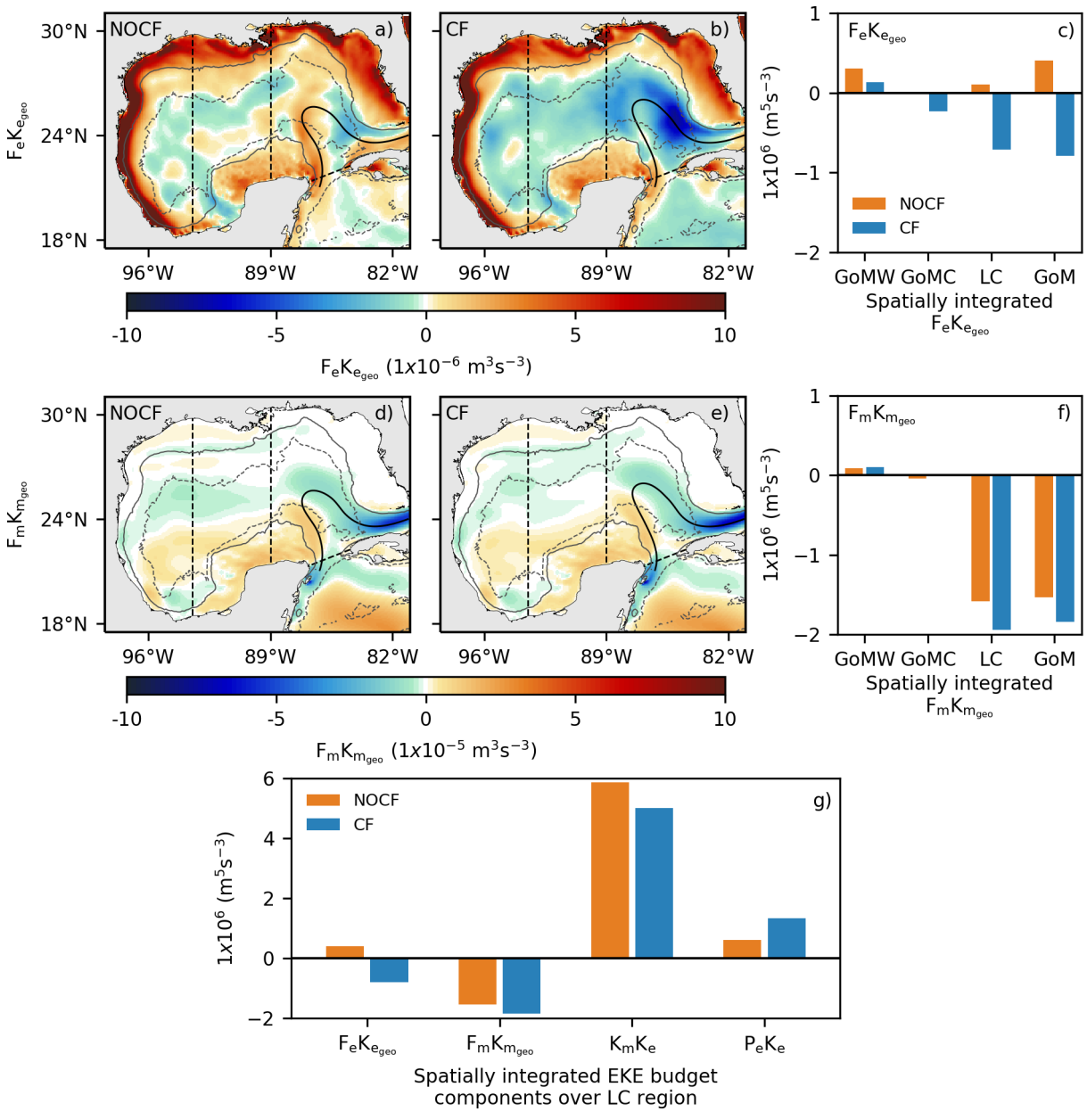

FIG. 6. Eddy (top) and mean (center) geostrophic wind work maps and spatially integrated values over regions (right) for the NOCF and CF experiments for the period 1993–2016. The segmented lines delimit the LC (east), center (GoMC) and west (GoMW) regions. GoM makes reference to the whole Gulf of Mexico. The light gray contours refers to the 200 (continuous) and 2500 m (segmented) depths. Spatially integrated energy budget terms over the LC region are shown in last panel (g).

Accepted for publication in *Journal of Physical Oceanography*. DOI 10.1175/JPO-D-21-0271.1.

The geostrophic mean wind work ($F_{\mathrm{m}}K_{\mathrm{m_g}}$) is a slightly larger in CF (Fig. 6d,e) because the LC mean penetration into the GoM is also larger when the CF is taken into account (Fig. 2). Notwithstanding, in comparison with NOCF, CFB drives up to 55% more energy to the atmosphere in $F_{\mathrm{e}}K_{\mathrm{e_g}}$ than in $F_{\mathrm{m}}K_{\mathrm{m_g}}$.

To sum up for the LC area, CFB reduces the production of EKE related to the horizontal shear of the currents (barotropic instabilities), which is partially compensated by increased baroclinic instabilities. Furthermore, CFB acts as an eddy killer by inducing a negative $F_{\mathrm{e}}K_{\mathrm{eg}}$ that damps the EKE.

4. Sensitivity of the Loop Current extension in the Gulf of Mexico

CFB acts on the circulation through two direct effects: a slow down of the mean circulation and a damping of the mesoscale activity. This sections aims to assess how these changes have impact the LC characteristics and in particular the LC energetics and its penetration into the GoM.

The LC penetration is generally described as a function of its extension and has been cataloged into retracted and extended forms (Garcia-Jove et al. 2016; Putrasahan et al. 2017). The retracted form is generally representative of a LC that has shed an eddy shortly before. In contrast, the extended form is representative of a LC that deeply penetrates the GoM and is about to shed an eddy. Figure 7 depicts the Probability Density Function (PDF) of the LC penetration into the GoM (binned into 0.1° boxes) from AVISO and the simulations. Three categories of LC penetration can in fact be identified: retracted, canonical and elongated (Fig. 7). The extended form found in the literature can be split into a canonical and elongated form. The canonical form, identified as the dominant mode in AVISO, NOCF, and CF (50.4%, 48.5%, and 51.1% of occurrence, respectively), can be located as the relative maximum near the Mississippi Fan (Figs. 7a-c). In contrast, the elongated form consists in an anomalous westward extension spreading beyond the Mississippi Fan. The elongated form occurs roughly 24% of the time in AVISO. Both simulations underestimate the occurrence of the elongated form. However, its representation is improved from NOCF to CF (from 2.7% in NOCF to 9.5% in CF) with respect to AVISO (24%), consistent with the more extended mean LC extension. They also overestimate the retracted form occurrence despite some improvement from NOCF to CF (25.6% in AVISO *vs.* 49.2% NOCF and 34.4% in CF), which can be identified as the relative maximum located east of the Campeche Bank. In addition, it is worth

Accepted for publication in *Journal of Physical Oceanography*. DOI 10.1175/JPO-D-21-0271.1

mentioning that the surface KE integrated over the LC is reduced by about 20% when considering CFB (Figs. 7d-f).

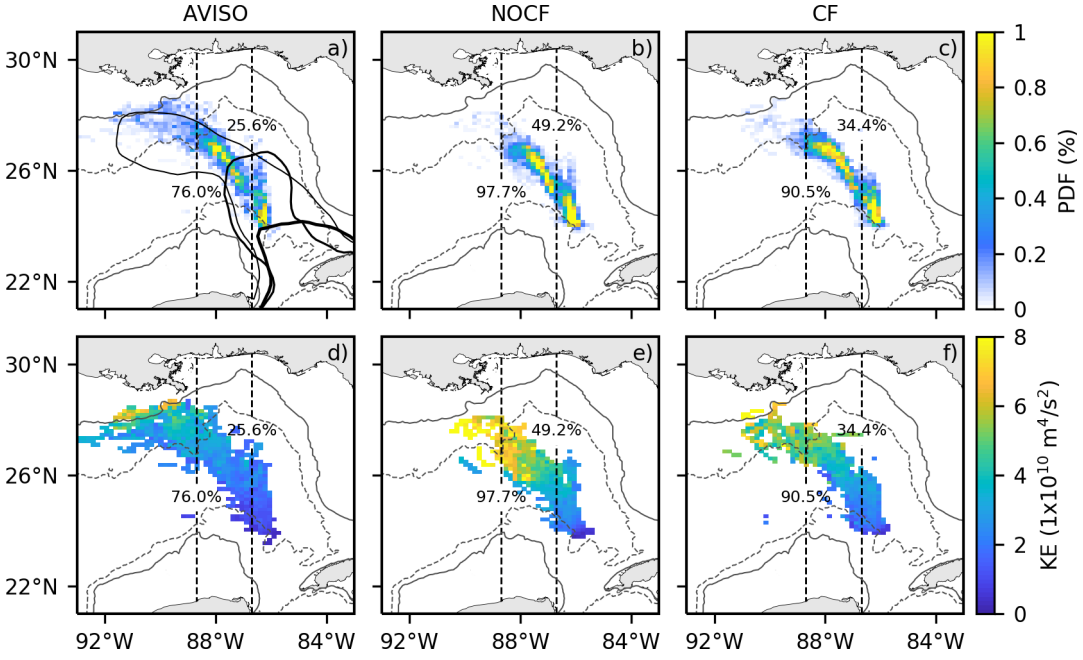

FIG. 7. Probability density functions related to the occurrence of LC maximum latitudes and longitudes for the period 1993–2016 for AVISO (first column), NOCF (second column) and CF (third column), and associated average of spatially integrated KE. The thick, medium–thick, and thin black contours represent examples of the retracted, canonical and elongated LC forms, respectively. The light gray contours refers to the 200 (continuous) and 2500 m (segmented) depths.

The reasons for this sensitivity are difficult to determine but several works propose that the LC extension is related to energy exchange between the GoM and the Caribbean Sea. On the one hand, Le Hénaff et al. (2012) and Garcia-Jove et al. (2016) show a relationship between the mesoscale activity over the Caribbean Sea and the LC penetration into the GoM: the weaker the EKE over the Cayman Sea, the more extended the LC. From NOCF to CF, there is a 27% EKE reduction over the Caribbean Sea (not shown) that would be in line with an increased extension of the LC in CF. However, a more considerable LC penetration into the GoM would be expected given this large EKE reduction. On the other hand, several studies suggest a possible relationship between the LC extension and the transport in the Yucatan Channel (Lin et al. 2010; Le Hénaff et al. 2012; Mildner

Accepted for publication in *Journal of Physical Oceanography*. DOI 10.1175/JPO-D-21-0271.1

et al. 2013; Athié et al. 2015, 2020). No such relationship was found in this study since the mean transport in the Yucatan Channel only reduced by 3% (27.4 Sv in CF and 26.6 Sv in NOCF).

5. Sensitivity of the Loop Current eddy shedding statistics and properties by the current feedback

LC eddies are responsible for transporting warm and salty water to the western region of the GoM. In a numerical simulation, it is therefore crucial to properly represent them in order to obtain realistic air-sea heat fluxes and thermohaline properties of the GoM. The goal of this section is therefore to evaluate the extent to which CFB modulates the LC eddy shedding process and the characteristics of the LC eddies during their journey within the GoM. To that end, the LC eddies detachment position and trajectory, as well as the properties related to their lifetime, energy, and vertical structure are assessed.

a. Number of detachments and separations

Long term statistics related to the LC eddy shedding are performed for AVISO, NOCF, and CF for the period 1993–2016. The timing of the eddy shedding is inferred by the inspection of daily SSHa fields and 17 cm SSHa contours length (Leben 2005; Garcia-Jove et al. 2016; Putrasahan et al. 2017). LC eddy shedding can result both in a reattachment when it is reincorporated to the LC, but also in a separation when the eddy travels westward and never reattach. Throughout the period of interest (1993–2016), a total of 61 detached eddies are identified in AVISO, from which 35 become separations (Table 2). While the number of detachments is similar in both simulations (55 in NOCF and 48 in CF) and compare relatively well with AVISO, there are large differences in terms of separation events. Indeed, not considering CFB leads to an under-representation of the number of separation events (only 16 in NOCF *vs.* 30 in CF) and to an overestimation of the time between separations (Fig. 8).

Accepted for publication in *Journal of Physical Oceanography*. DOI 10.1175/JPO-D-21-0271.1

TABLE 2. Statistics related to the LC eddies shedding and their detection through the eddy detection method (EDM). Number of detached LC eddies (first column). Number of LC eddies that are nor reabsorbed by the LC and travel to the west of the GoM (second column). Number of separated eddies detected by the eddy detection method (EDM; third column). Number of separated eddies detected by the eddy detection method (EDM) with a lifetime longer than 200 days (forth column).

	Detachments	Separations	Separated eddies detected by the EDM	Lifetime longer than 200 days
AVISO	61	35	31	21
CF	55	30	30	26
NOCF	48	16	16	14

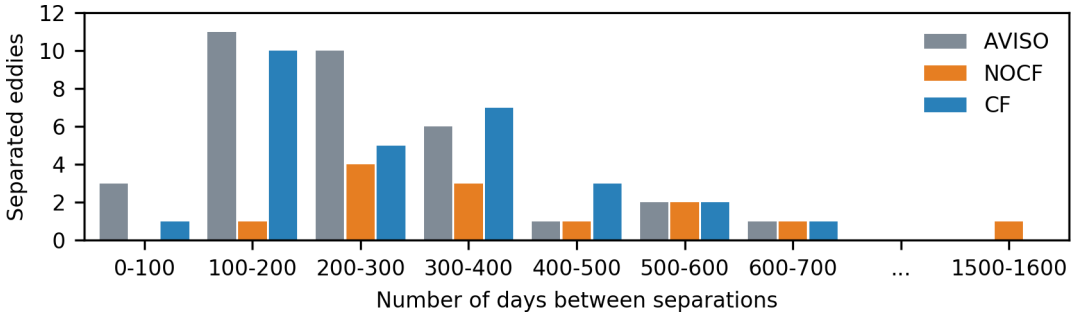

FIG. 8. Number of separated LC eddies as a function of the number of days between separations.

b. Latitude of the eddy separation

The modulation of eddy shedding properties from NOCF to CF may be due to an alteration of the localization of the eddy separation. By ignoring CFB, NOCF favors LC eddies liberation farther south (between 88.6–87.0°W and 25.2–26.5°N; Fig. 9c), which is likely related to the over–representation of the LC retracted form in NOCF. In contrast, in CF, CFB causes higher elongated occurrence of the LC and a weaker EKE in the LC area, and, thus, eddy detachment and statistics more realistic with respect to AVISO. The impact of CFB on the latitude of detachment is further confirmed by analyzing the outermost position of the LC during separation events (Fig. 10). For each experiment and AVISO, a meridional PDF is computed by grouping the estimated outermost positions of the LC after a separation event for each degree of latitude (Figs. 10d,h; note that resizing the boxes between 0.4 and 1.5° does not change the results significantly). The

Accepted for publication in *Journal of Physical Oceanography*. DOI 10.1175/JPO-D-21-0271.1.

25–26°N latitude range remains the preferential latitudes of separation for AVISO and for both simulations. However, in AVISO, more than 77% of the separations (27 cases) occur north of 25°N, while this ratio falls to 39% (12 cases) in CF and 49% (8 cases) in NOCF. The distributions reveal that in NOCF, both distributions of separations and reattachments are skewed toward the south (Figs. 10d,h). Including CFB leads to a more realistic LC extension and LC eddy separation events, but also to a decrease in the excessive number of reattachment from the south of the LC.

Accepted for publication in *Journal of Physical Oceanography*. DOI 10.1175/JPO-D-21-0271.1.

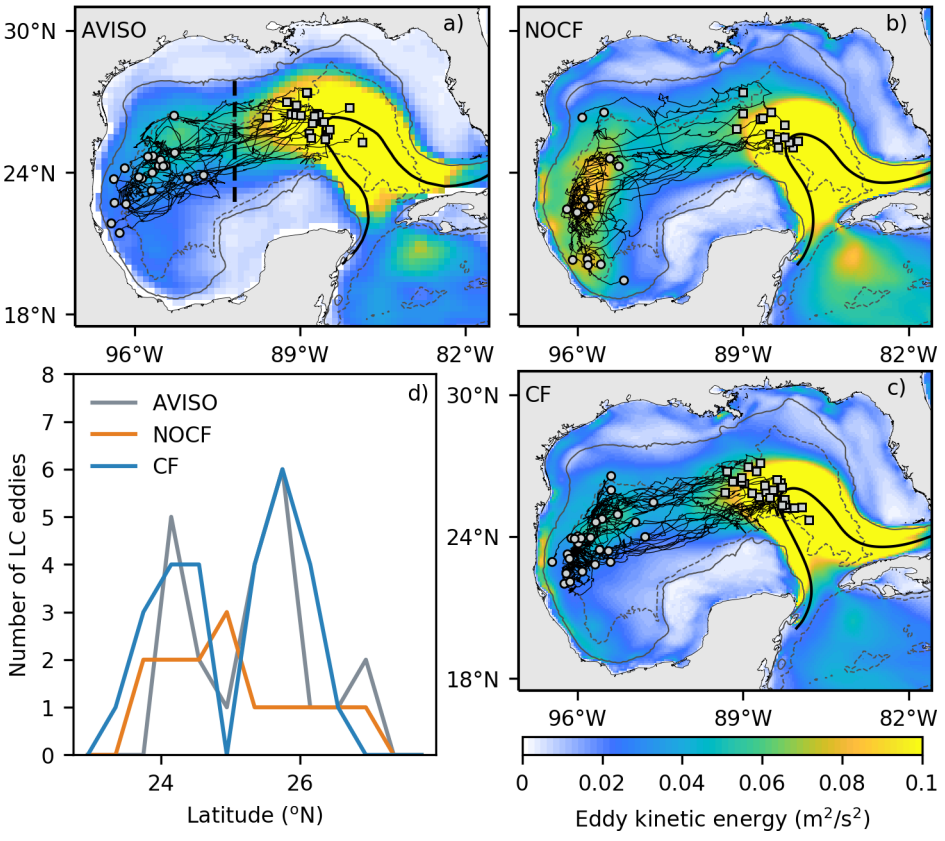

FIG. 9. Trajectories related to LC eddies with a lifetime longer than 200 days for AVISO (a), NOCF (b), and CF (c). Gray squares represent the location of a LC eddy liberation, and gray circles the location where LC eddies are no longer detected. The colormap refers to the corresponding EKE climatology. The 17 cm contours of the climatological sea surface height anomaly of AVISO and the numerical experiments are represented by the black line. The light gray contours refers to the 200 (continuous) and 2500 m (segmented) depths. (d) Number of LC eddies that cross the segmented thick line shown in panel a) as a function of the latitude.

Accepted for publication in *Journal of Physical Oceanography*. DOI 10.1175/JPO-D-21-0271.1.

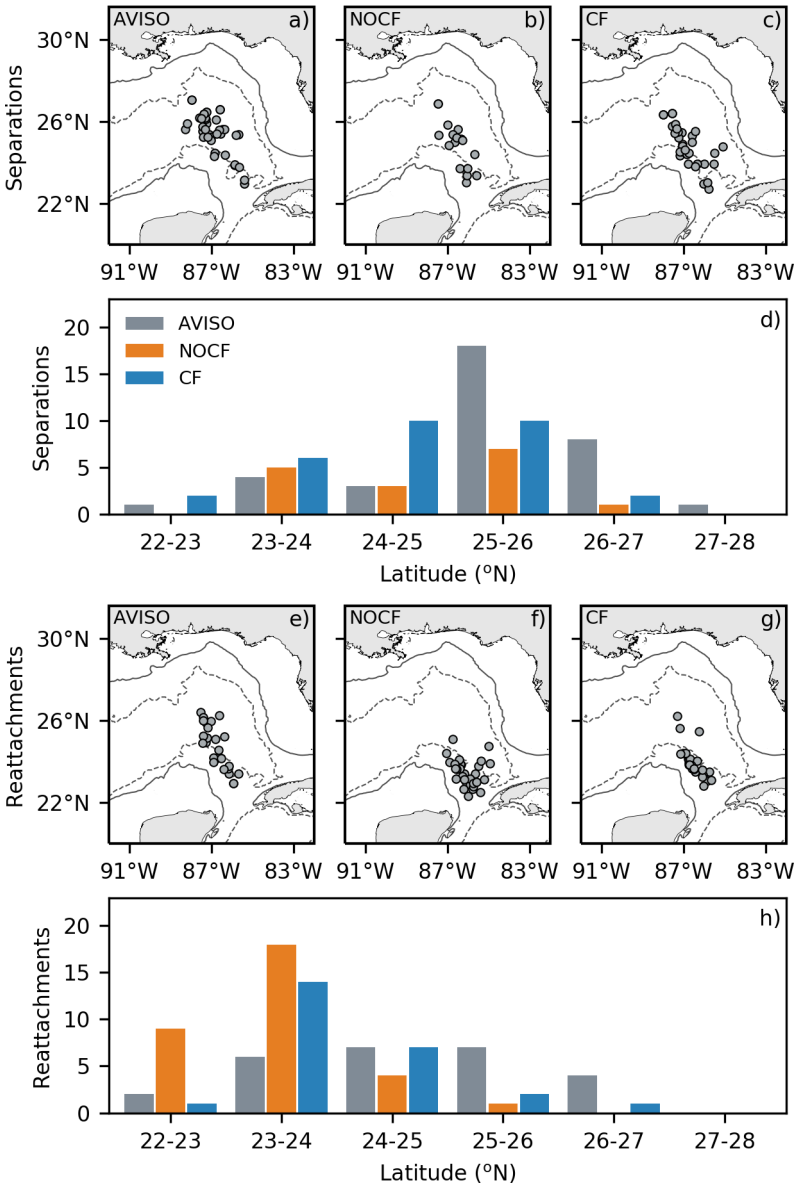

FIG. 10. LC most extended position (gray dots) after separation (first row) and reattachment (second row) events, for AVISO (first column), NOCF (second column) and CF (third column). The light gray contours refers to the 200 (continuous) and 2500 m (segmented) depths. PDFs related to the latitude of the LC most extended position after a separation and reattachment events are show in g) and h).

Accepted for publication in *Journal of Physical Oceanography*. DOI 10.1175/JPO-D-21-0271.1.

c. LC eddy trajectories and properties

To investigate further the impact of CFB on the LC eddies, statistics on the long–lived detected eddies (lifetime longer than 3 months as in Sosa-Gutiérrez et al. 2020; Chelton et al. 2011) are assessed in the following.

In both simulations and in AVISO, LC eddies preferentially travel southwestward along a vortex street located between 24°N and 26°N (Fig. 9). CFB clearly alters the LC eddies and therefore the vortex street position, improving the realism of the simulations. Two main effects can be distinguished. On the one hand, likely because of the too south location of the eddy shedding, the vortex street in NOCF is shifted toward the south and mainly restricted between 23–26°N (Fig. 9d). On the other hand, consistent with the eddy killing and the subsequent damping of the EKE, CFB largely impacts the eddy lifetime and fate in the western GoM. Eddy energy is reduced from NOCF to CF by 24% (Table 3), and LC eddies in NOCF have a larger KE dissipation rate with respect to that in CF. On average, LC eddies lifetime is also shorten by about 16% (528 days in average in NOCF *vs.* 445 days in CF and 377 in AVISO). As in Renault et al. (2016b) for the US West coast, the overestimation of the eddy lifetime in NOCF allows the LC eddies to travel unrealistically too far in the Bay of Campeche (south of 22°N). Finally, CFB does not have a significant impact on the translation speed of the LC eddies (about 4 km/day in both simulations; Table 3).

TABLE 3. Statistics of LC eddies properties with a lifetime longer than 200 days.

	Lifetime (days)	Translation velocity (km/day)	EKE (m^2s^{-2})	EKE dissipation rate ($1x10^{-4}$ m^2s^{-2}/day)
AVISO	377 ± 118	4.59 ± 0.71	0.13 ± 0.05	-3.00 ± 1.36
CF	445 ± 126	4.14 ± 0.58	0.25 ± 0.06	-4.00 ± 1.70
NOCF	528 ± 179	4.37 ± 0.53	0.33 ± 0.14	-5.00 ± 2.24

d. LC eddies vertical structure

CFB affects in a profound way LC eddies. Indeed, besides the alteration of their life time and fate, their 3D structure is also impacted by CFB. The composites of long–lived LC eddies thermohaline and vorticity structure from NOCF and CF are shown in Fig. 11. The vertical structure of the LC eddies composite in CF is in good agreement with the observations of Elliott (1982) and Meunier et al. (2018, 2021). LC eddy composite is characterized by a warm and relative fresh core (between

Accepted for publication in *Journal of Physical Oceanography*. DOI 10.1175/JPO-D-21-0271.1

20 and 25°C and 36.5 PSU) well delimited by a superficial and a deeper thermocline (Figure 11d). In NOCF, the eddy composite has a warmer and saltier core and the upper thermocline goes deeper at the center of the eddy (Figure 11a,b). The deepening of the surface thermocline in NOCF is likely related to a larger negative vorticity at the eddy core (Figure 11c). Additionally, in NOCF, the salinity in the eddy core is uniform, and does not exhibit a minimum of salinity between 50 and 100 m, which is present in both the observations (Elliott 1982; Meunier et al. 2018, 2021) and CF.

Accepted for publication in *Journal of Physical Oceanography*. DOI 10.1175/JPO-D-21-0271.1.

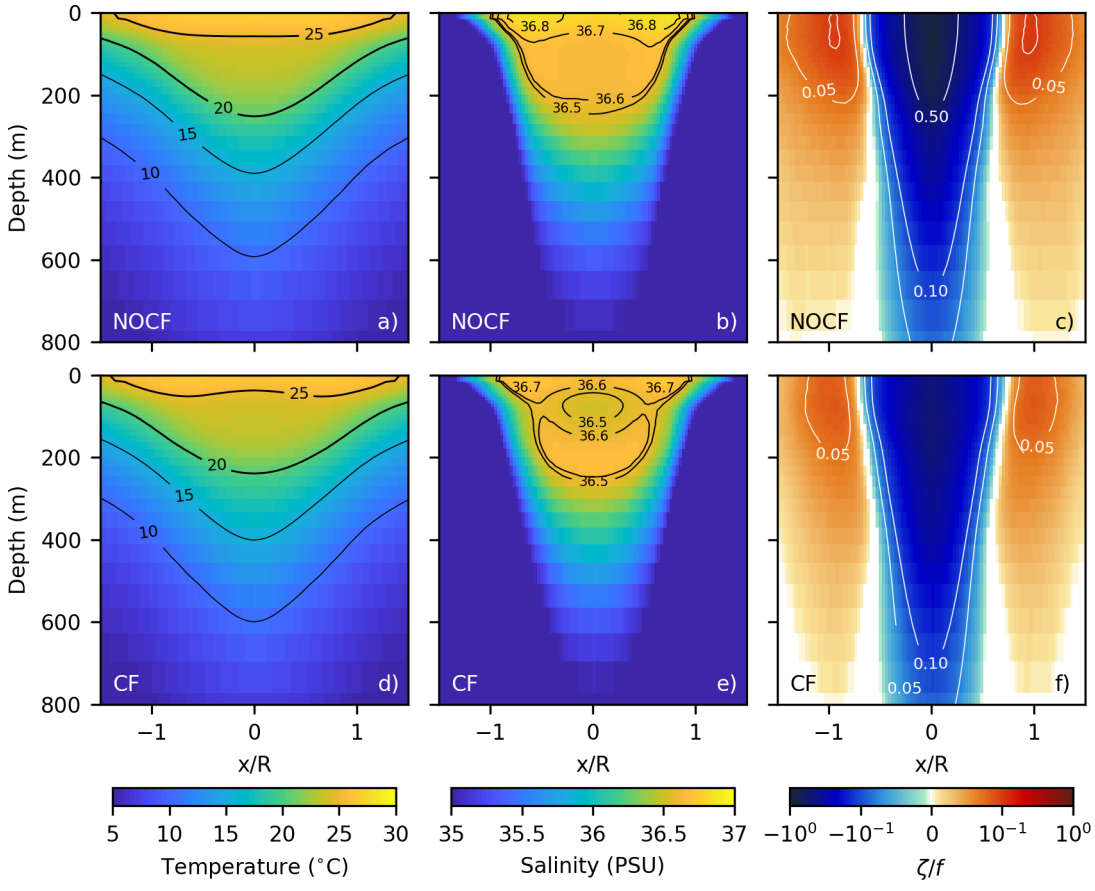

FIG. 11. LC eddy composite of temperature (first column) and salinity (second column) and the relative vorticity (ζ) normalized with the Coriolis parameter (f; third column) for CF (first row) and NOCF (second row). Black and thick contours indicate thermoclines at 26 and 220 m depth. Normalized relative vorticity contours of 0.05, 0.1 and 0.5 are shown using white lines.

6. Discussion and conclusions

Using long-term regional ocean-atmosphere coupled simulations with and without CFB, we assess to which extent CFB modulates the GoM dynamics. Consistent with previous studies over other regions, as a direct effect, CFB causes a damping of 20% of the mesoscale activity over the GoM. This reduction of mesoscale activity is mainly driven by the eddy killing mechanism, *i.e.*, a deflection of momentum from the mesoscale surface current to the atmosphere, and, to a lesser degree, by a reduction of the barotropic conversion of energy that is only partly compensated by an increase of the baroclinic conversion. As an indirect effect, taking into account CFB in a coupled model leads to an improvement of the representation of the LC dynamic. CFB alters the mean

Accepted for publication in *Journal of Physical Oceanography*. DOI 10.1175/JPO-D-21-0271.1.

LC extension, favoring its western penetration into the GoM. Using satellites observations and the simulations, we show that the LC extension can be classified into three categories: retracted, canonical and elongated. Both simulations underestimate the elongated form occurrence and over-represent the retracted form, although, consistent with the increase of the mean LC extension, CFB leads to a higher (lower) occurrence of the elongated (retracted) form.

The over–representation of the LC retracted form in NOCF could result in the reattachment of LC eddies that are detached from the south of the LC, since their path to the west of the GoM could be blocked by the Campeche Bank. In contrast, CFB favors a larger extension of the LC, allowing eddy shedding in the north and upper north regions of the LC and avoiding a large number of reattachments in the south. Besides, by increasing the LC eddy detachments from northern latitudes, LC eddies trajectories are not skewed toward to the south and become more similar to those observed in AVISO.

CFB also lead to a better representation of LC eddy properties. In particular, the vertical distribution of thermohaline properties of LC eddies are in better agreement with hydrographic (Elliott 1982) and gliders (Meunier et al. 2018, 2021) observations. In a simulation without CFB, LC eddies are too energetic, which leads to a deepening of the superficial thermocline, and to an increase of their heat content. The lack of sink of energy from mesoscale currents to the atmosphere also leads to an overestimation of LC eddies lifetime and to a poor estimation of their propagation. This may be critical to better represent extreme atmospheric events, as LC eddies can participate to an increase the occurrence of thunderstorms and tornado events in the Southeast U.S., as well as the reinforcement of hurricanes (Molina et al. 2016; Yablonsky and Ginis 2012).

This study is the first to show that CFB has important consequences on the GoM dynamics and LC eddy shedding. Given the dramatic consequences of CFB on the GoM dynamics, is the uncoupled approach no longer suitable and are we doomed to use a coupled model to simulate the GoM oceanic circulation? Following Renault et al. (2020) can be parameterized using a wind or a stress correction approach. This has been done successfully at an almost global scale by Renault et al. (2020) and for the U.S. West coast by Renault et al. (2021b), but should be tested for the GoM. To conclude, the coupled simulation with CFB used in this study still suffers from biases. For instance, LC penetration into the GoM, although improved, is still underestimated. This could be due to the prescribed oceanic conditions at the open boundary of the simulation, but also to missing

Accepted for publication in *Journal of Physical Oceanography*. DOI 10.1175/JPO-D-21-0271.1

physical processes. In particular, wave feedbacks to the ocean and the atmosphere may modulate the ocean energy budget and the transfer of energy between the ocean and the atmosphere. This could modulate the GoM dynamics and the role of CFB in determining it.

Finally, current satellite products do not allow for an accurate characterization of the surface current, the surface stress response to CFB and thereby the wind work (Renault et al. 2017a). While future satellite missions such as SWOT (Morrow et al. 2019) will allow measuring the geostrophic currents with a better spatial resolution than the current observations, likely allowing to resolve the mesoscale activity, coherent measurements of total current and surface stress will be still be missing. Future Satellite missions projects such as WaCM (Wind and Current Measurments; Bourassa et al. 2016; Rodríguez et al. 2019) should overcome this issue, this would help to better understand the wind work, the air-sea interactions, the energy pathway in the ocean and more generally to better constrain and validate numerical models.

Accepted for publication in *Journal of Physical Oceanography*. DOI 10.1175/JPO-D-21-0271.1

Acknowledgments. The PhD grant of ML was supported by CNES and Université Paul Sabatier. Supercomputing facilities were provided by GENCI project GEN7298 and GEN13051. The authors appreciate support from the CNES (Projects CARAMBA and I–CASCADE) and the ANR JPI-CLIMATE EUREC4A-OA.

Data availability statement. All presented data are available at 10.6084/m9.figshare.17032367

References

Amores, A., G. Jordà, T. Arsouze, and J. Le Sommer, 2018: Up to what extent can we characterize ocean eddies using present-day gridded altimetric products? *Journal of Geophysical Research: Oceans*, **123 (10)**, 7220–7236.

Archer, M. R., Z. Li, and L.-L. Fu, 2020: Increasing the space–time resolution of mapped sea surface height from altimetry. *Journal of Geophysical Research: Oceans*, **125 (6)**, https://doi.org/10.1029/2019jc015878, URL https://doi.org/10.1029/2019jc015878.

Athié, G., J. Sheinbaum, J. Candela, J. Ochoa, P. Pérez-Brunius, and A. Romero-Arteaga, 2020: Seasonal variability of the transport through the yucatan channel from observations. *Journal of Physical Oceanography*, **50 (2)**, 343–360, https://doi.org/10.1175/jpo-d-18-0269.1, URL https://doi.org/10.1175/jpo-d-18-0269.1.

Athié, G., J. Sheinbaum, R. Leben, J. Ochoa, M. R. Shannon, and J. Candela, 2015: Interannual variability in the yucatan channel flow. *Geophysical Research Letters*, **42 (5)**, 1496–1503, https://doi.org/10.1002/2014gl062674, URL https://doi.org/10.1002/2014gl062674.

Bourassa, M. A., E. Rodriguez, and D. Chelton, 2016: Winds and currents mission: Ability to observe mesoscale AIR/SEA coupling. *2016 IEEE International Geoscience and Remote Sensing Symposium (IGARSS)*, IEEE, https://doi.org/10.1109/igarss.2016.7730928, URL https://doi.org/10.1109/igarss.2016.7730928.

Bye, J. A., 1985: Chapter 6 large-scale momentum exchange in the coupled atmosphere-ocean. *Elsevier oceanography series*, Elsevier, 51–61, https://doi.org/10.1016/s0422-9894(08)70702-5, URL https://doi.org/10.1016/s0422-9894(08)70702-5.

Accepted for publication in *Journal of Physical Oceanography*. DOI 10.1175/JPO-D-21-0271.1

Candela, J., J. Sheinbaum, J. Ochoa, A. Badan, and R. Leben, 2002: The potential vorticity flux through the yucatan channel and the loop current in the gulf of mexico. *Geophysical Research Letters*, **29 (22)**, 16–1–16–4, https://doi.org/10.1029/2002gl015587, URL https://doi.org/10.1029/2002gl015587.

Chaigneau, A., G. Eldin, and B. Dewitte, 2009: Eddy activity in the four major upwelling systems from satellite altimetry (1992–2007). *Progress in Oceanography*, **83 (1-4)**, 117–123.

Chang, Y.-L., and L.-Y. Oey, 2013: Loop current growth and eddy shedding using models and observations: Numerical process experiments and satellite altimetry data. *Journal of Physical Oceanography*, **43 (3)**, 669–689, https://doi.org/10.1175/jpo-d-12-0139.1, URL https://doi.org/10.1175/jpo-d-12-0139.1.

Chelton, D. B., M. G. Schlax, and R. M. Samelson, 2011: Global observations of nonlinear mesoscale eddies. *Progress in Oceanography*, **91 (2)**, 167–216, https://doi.org/https://doi.org/10.1016/j.pocean.2011.01.002, URL https://www.sciencedirect.com/science/article/pii/S0079661111000036.

Chen, F., and J. Dudhia, 2001: Coupling an advanced land surface–hydrology model with the penn state–ncar mm5 modeling system. part i: Model implementation and sensitivity. *Monthly weather review*, **129 (4)**, 569–585.

Coronado, C., J. Candela, R. Iglesias-Prieto, J. Sheinbaum, M. López, and F. J. Ocampo-Torres, 2007: On the circulation in the puerto morelos fringing reef lagoon. *Coral Reefs*, **26 (1)**, 149–163, https://doi.org/10.1007/s00338-006-0175-9, URL https://doi.org/10.1007/s00338-006-0175-9.

Cuevas, E., A. Uribe-Martínez, and M. de los Ángeles Liceaga-Correa, 2018: A satellite remote-sensing multi-index approach to discriminate pelagic sargassum in the waters of the yucatan peninsula, mexico. *International Journal of Remote Sensing*, **39 (11)**, 3608–3627, https://doi.org/10.1080/01431161.2018.1447162, URL https://doi.org/10.1080/01431161.2018.1447162.

Damien, P., J. Sheinbaum, O. Pasqueron de Fommervault, J. Jouanno, L. Linacre, and O. Duteil, 2021: Do loop current eddies stimulate productivity in the gulf of mexico? *Biogeosciences Discussions*, 1–52.

Accepted for publication in *Journal of Physical Oceanography*. DOI 10.1175/JPO-D-21-0271.1

Dussin, R., B. Barnier, L. Brodeau, and J. M. Molines, 2016: The making of the drakkar forcing set dfs5. *DRAKKAR/MyOcean Rep*, **104**, 16.

Elliott, B. A., 1982: Anticyclonic rings in the gulf of mexico. *Journal of Physical Oceanography*, **12 (11)**, 1292–1309, https://doi.org/10.1175/1520-0485(1982)012<1292:aritgo>2.0.co;2, URL https://doi.org/10.1175/1520-0485(1982)012<1292:aritgo>2.0.co;2.

Fratantoni, P. S., T. N. Lee, G. P. Podesta, and F. Muller-Karger, 1998: The influence of loop current perturbations on the formation and evolution of tortugas eddies in the southern straits of florida. *Journal of Geophysical Research: Oceans*, **103 (C11)**, 24 759–24 779, https://doi.org/10.1029/98jc02147, URL https://doi.org/10.1029/98jc02147.

Garcia-Jove, M., , J. Sheinbaum, J. Jouanno, and and, 2016: Sensitivity of loop current metrics and eddy detachments to different model configurations: The impact of topography and caribbean perturbations. *Atmósfera*, **29 (3)**, 235–265, https://doi.org/10.20937/atm.2016.29.03.05, URL https://doi.org/10.20937/atm.2016.29.03.05.

Gévaudan, M., J. Jouanno, F. Durand, G. Morvan, L. Renault, and G. Samson, 2021: Influence of ocean salinity stratification on the tropical atlantic ocean surface. *Climate Dynamics*, https://doi.org/10.1007/s00382-021-05713-z, URL https://doi.org/10.1007/s00382-021-05713-z.

Gower, J., C. Hu, G. Borstad, and S. King, 2006: Ocean color satellites show extensive lines of floating sargassum in the gulf of mexico. *IEEE Transactions on Geoscience and Remote Sensing*, **44 (12)**, 3619–3625, https://doi.org/10.1109/tgrs.2006.882258, URL https://doi.org/10.1109/tgrs.2006.882258.

Gower, J. F. R., and S. A. King, 2011: Distribution of floating sargassum in the gulf of mexico and the atlantic ocean mapped using MERIS. *International Journal of Remote Sensing*, **32 (7)**, 1917–1929, https://doi.org/10.1080/01431161003639660, URL https://doi.org/10.1080/01431161003639660.

Hiron, L., B. J. Cruz, and L. K. Shay, 2020: Evidence of loop current frontal eddy intensification through local linear and nonlinear interactions with the loop current. *Jour-*

Accepted for publication in *Journal of Physical Oceanography*. DOI 10.1175/JPO-D-21-0271.1.

nal of Geophysical Research: Oceans, **125 (4)**, https://doi.org/10.1029/2019jc015533, URL https://doi.org/10.1029/2019jc015533.

Hong, S.-Y., 2010: A new stable boundary-layer mixing scheme and its impact on the simulated east asian summer monsoon. *Quarterly Journal of the Royal Meteorological Society*, **136 (651)**, 1481–1496.

Hong, S.-Y., and J. O. J. Lim, 2006: The wrf single-moment 6-class microphysics scheme (wsm6). *J. Korean Meteor. Soc.*, **42**, 129–151.

Hong, S.-Y., Y. Noh, and J. Dudhia, 2006: A new vertical diffusion package with an explicit treatment of entrainment processes. *Monthly weather review*, **134 (9)**, 2318–2341.

Hurlburt, H. E., and J. D. Thompson, 1980: A numerical study of loop current intrusions and eddy shedding. *Journal of Physical Oceanography*, **10 (10)**, 1611–1651, https://doi.org/10.1175/1520-0485(1980)010<1611:ansolc>2.0.co;2, URL https://doi.org/10.1175/1520-0485(1980)010<1611:ansolc>2.0.co;2.

Iacono, M. J., J. S. Delamere, E. J. Mlawer, M. W. Shephard, S. A. Clough, and W. D. Collins, 2008: Radiative forcing by long-lived greenhouse gases: Calculations with the aer radiative transfer models. *Journal of Geophysical Research: Atmospheres*, **113 (D13)**.

Jouanno, J., J. Ochoa, E. Pallàs-Sanz, J. Sheinbaum, F. Andrade-Canto, J. Candela, and J.-M. Molines, 2016: Loop current frontal eddies: Formation along the campeche bank and impact of coastally trapped waves. *Journal of Physical Oceanography*, **46 (11)**, 3339–3363, https://doi.org/10.1175/jpo-d-16-0052.1, URL https://doi.org/10.1175/jpo-d-16-0052.1.

Jullien, S., S. Masson, V. Oerder, G. Samson, F. Colas, and L. Renault, 2020: Impact of ocean–atmosphere current feedback on ocean mesoscale activity: Regional variations and sensitivity to model resolution. *Journal of Climate*, **33 (7)**, 2585–2602, https://doi.org/10.1175/jcli-d-19-0484.1, URL https://doi.org/10.1175/jcli-d-19-0484.1.

Kostka, J. E., and Coauthors, 2011: Hydrocarbon-degrading bacteria and the bacterial community response in gulf of mexico beach sands impacted by the deepwater horizon oil spill. *Applied and Environmental Microbiology*, **77 (22)**, 7962–7974, https://doi.org/10.1128/aem.05402-11, URL https://doi.org/10.1128/aem.05402-11.

Le Hénaff, M., V. H. Kourafalou, Y. Morel, and A. Srinivasan, 2012: Simulating the dynamics and intensification of cyclonic loop current frontal eddies in the gulf of mexico. *Journal of Geophysical Research: Oceans*, **117 (C2)**, n/a–n/a, https://doi.org/10.1029/2011jc007279, URL https://doi.org/10.1029/2011jc007279.

Leben, R. R., 2005: Altimeter-derived loop current metrics. *Geophysical Monograph-American Geophysical Union*, **161**, 181.

Lellouche, J.-M., and Coauthors, 2018: Recent updates to the copernicus marine service global ocean monitoring and forecasting real-time 1/12° high-resolution system. *Ocean Science*, **14 (5)**, 1093–1126, https://doi.org/10.5194/os-14-1093-2018, URL https://doi.org/10.5194/os-14-1093-2018.

Lemarié, F., E. Blayo, and L. Debreu, 2015: Analysis of ocean-atmosphere coupling algorithms: Consistency and stability. *Procedia Computer Science*, **51**, 2066–2075, https://doi.org/10.1016/j.procs.2015.05.473, URL https://doi.org/10.1016/j.procs.2015.05.473.

Lin, Y., R. J. Greatbatch, and J. Sheng, 2010: The influence of gulf of mexico loop current intrusion on the transport of the florida current. *Ocean Dynamics*, **60 (5)**, 1075–1084, https://doi.org/10.1007/s10236-010-0308-0, URL https://doi.org/10.1007/s10236-010-0308-0.

Luo, J.-J., S. Masson, E. Roeckner, G. Madec, and T. Yamagata, 2005: Reducing climatology bias in an ocean–atmosphere CGCM with improved coupling physics. *Journal of Climate*, **18 (13)**, 2344–2360, https://doi.org/10.1175/jcli3404.1, URL https://doi.org/10.1175/jcli3404.1.

Ma, X., and Coauthors, 2016: Western boundary currents regulated by interaction between ocean eddies and the atmosphere. *Nature*, **535 (7613)**, 533–537, https://doi.org/10.1038/nature18640, URL https://doi.org/10.1038/nature18640.

Madec, G., and N. S. Team, 2016: *NEMO ocean engine*. https://doi.org/10.5281/zenodo.1464816.

Marchesiello, P., J. C. McWilliams, and A. Shchepetkin, 2003: Equilibrium structure and dynamics of the california current system. *Journal of physical Oceanography*, **33 (4)**, 753–783.

Meunier, T., E. Pallás-Sanz, M. Tenreiro, E. Portela, J. Ochoa, A. Ruiz-Angulo, and S. Cusí, 2018: The vertical structure of a loop current eddy. *Journal of Geophysical Research:*

Accepted for publication in *Journal of Physical Oceanography*. DOI 10.1175/JPO-D-21-0271.1

Oceans, **123 (9)**, 6070–6090, https://doi.org/10.1029/2018jc013801, URL https://doi.org/10.1029/2018jc013801.

Meunier, T., E. P. Sanz, C. de Marez, J. Pérez, M. Tenreiro, A. R. Angulo, and A. Bower, 2021: The dynamical structure of a warm core ring as inferred from glider observations and along-track altimetry. *Remote Sensing*, **13 (13)**, 2456, https://doi.org/10.3390/rs13132456, URL https://doi.org/10.3390/rs13132456.

Meunier, T., J. Sheinbaum, E. Pallàs-Sanz, M. Tenreiro, J. Ochoa, A. Ruiz-Angulo, X. Carton, and C. de Marez, 2020: Heat content anomaly and decay of warm-core rings: the case of the gulf of mexico. *Geophysical Research Letters*, **47 (3)**, https://doi.org/10.1029/2019gl085600, URL https://doi.org/10.1029/2019gl085600.

Michel, J., and Coauthors, 2013: Extent and degree of shoreline oiling: Deepwater horizon oil spill, gulf of mexico, USA. *PLoS ONE*, **8 (6)**, e65 087, https://doi.org/10.1371/journal.pone.0065087, URL https://doi.org/10.1371/journal.pone.0065087.

Mildner, T. C., C. Eden, and L. Czeschel, 2013: Revisiting the relationship between loop current rings and florida current transport variability. *Journal of Geophysical Research: Oceans*, **118 (12)**, 6648–6657, https://doi.org/10.1002/2013jc009109, URL https://doi.org/10.1002/2013jc009109.

Mlawer, E. J., S. J. Taubman, P. D. Brown, M. J. Iacono, and S. A. Clough, 1997: Radiative transfer for inhomogeneous atmospheres: Rrtm, a validated correlated-k model for the longwave. *Journal of Geophysical Research: Atmospheres*, **102 (D14)**, 16 663–16 682.

Molina, M. J., R. P. Timmer, and J. T. Allen, 2016: Importance of the gulf of mexico as a climate driver for u.s. severe thunderstorm activity. *Geophysical Research Letters*, **43 (23)**, https://doi.org/10.1002/2016gl071603, URL https://doi.org/10.1002/2016gl071603.

Morrow, R., and Coauthors, 2019: Global observations of fine-scale ocean surface topography with the surface water and ocean topography (swot) mission. *Frontiers in Marine Science*, **6**, 1–19.

Oerder, V., F. Colas, V. Echevin, S. Masson, and F. Lemarié, 2018: Impacts of the mesoscale ocean-atmosphere coupling on the peru-chile ocean dynamics: The current-induced wind stress

Accepted for publication in *Journal of Physical Oceanography*. DOI 10.1175/JPO-D-21-0271.1.

modulation. *Journal of Geophysical Research: Oceans*, **123 (2)**, 812–833, https://doi.org/10.1002/2017jc013294, URL https://doi.org/10.1002/2017jc013294.

Oey, L.-Y., 2008: Loop current and deep eddies. *Journal of Physical Oceanography*, **38 (7)**, 1426–1449, https://doi.org/10.1175/2007jpo3818.1, URL https://doi.org/10.1175/2007jpo3818.1.

Pacanowski, R. C., 1987: Effect of equatorial currents on surface stress. *Journal of physical oceanography*, **17 (6)**, 833–838, https://doi.org/10.1175/1520-0485(1987)017<0833:eoecos>2.0.co;2, URL https://doi.org/10.1175/1520-0485(1987)017<0833:eoecos>2.0.co;2.

Pegliasco, C., A. Chaigneau, and R. Morrow, 2015: Main eddy vertical structures observed in the four major eastern boundary upwelling systems. *Journal of Geophysical Research: Oceans*, **120 (9)**, 6008–6033.

Phillips, M. B., and T. H. Bonner, 2015: Occurrence and amount of microplastic ingested by fishes in watersheds of the gulf of mexico. *Marine Pollution Bulletin*, **100 (1)**, 264–269, https://doi.org/10.1016/j.marpolbul.2015.08.041, URL https://doi.org/10.1016/j.marpolbul.2015.08.041.

Pichevin, T., and D. Nof, 1997: The momentum imbalance paradox. *Tellus A*, **49 (2)**, 298–319, https://doi.org/10.1034/j.1600-0870.1997.t01-1-00009.x, URL https://doi.org/10.1034/j.1600-0870.1997.t01-1-00009.x.

Putrasahan, D. A., I. Kamenkovich, M. L. Hénaff, and B. P. Kirtman, 2017: Importance of ocean mesoscale variability for air-sea interactions in the gulf of mexico. *Geophysical Research Letters*, **44 (12)**, 6352–6362, https://doi.org/10.1002/2017gl072884, URL https://doi.org/10.1002/2017gl072884.

Reffray, G., R. Bourdalle-Badie, and C. Calone, 2015: Modelling turbulent vertical mixing sensitivity using a 1-d version of nemo. *Geoscientific Model Development*, **8 (1)**, 69–86, https://doi.org/10.5194/gmd-8-69-2015, URL https://gmd.copernicus.org/articles/8/69/2015/.

Renault, L., T. Arsouze, and J. Ballabrera-Poy, 2021a: On the influence of the current feedback to the atmosphere on the western mediterranean sea dynamics. *Journal of Geophysical Research: Oceans*, **126 (1)**, https://doi.org/10.1029/2020jc016664, URL https://doi.org/10.1029/2020jc016664.

Accepted for publication in *Journal of Physical Oceanography*. DOI 10.1175/JPO-D-21-0271.1.

Renault, L., F. Lemarié, and T. Arsouze, 2019a: On the implementation and consequences of the oceanic currents feedback in ocean–atmosphere coupled models. *Ocean Modelling*, **141**, 101 423, https://doi.org/10.1016/j.ocemod.2019.101423, URL https://doi.org/10.1016/j.ocemod.2019.101423.

Renault, L., P. Marchesiello, S. Masson, and J. C. Mcwilliams, 2019b: Remarkable control of western boundary currents by eddy killing, a mechanical air-sea coupling process. *Geophysical Research Letters*, **46 (5)**, 2743–2751.

Renault, L., S. Masson, T. Arsouze, G. Madec, and J. C. McWilliams, 2020: Recipes for how to force oceanic model dynamics. *Journal of Advances in Modeling Earth Systems*, **12 (2)**, https://doi.org/10.1029/2019ms001715, URL https://doi.org/10.1029/2019ms001715.

Renault, L., J. C. McWilliams, F. Kessouri, A. Jousse, H. Frenzel, R. Chen, and C. Deutsch, 2021b: Evaluation of high-resolution atmospheric and oceanic simulations of the california current system. *Progress in Oceanography*, **195**, 102 564, https://doi.org/10.1016/j.pocean.2021.102564, URL https://doi.org/10.1016/j.pocean.2021.102564.

Renault, L., J. C. McWilliams, and S. Masson, 2017a: Satellite observations of imprint of oceanic current on wind stress by air-sea coupling. *Scientific Reports*, **7 (1)**, https://doi.org/10.1038/s41598-017-17939-1, URL https://doi.org/10.1038/s41598-017-17939-1.

Renault, L., J. C. McWilliams, and P. Penven, 2017b: Modulation of the agulhas current retroflection and leakage by oceanic current interaction with the atmosphere in coupled simulations. *Journal of Physical Oceanography*, **47 (8)**, 2077–2100.

Renault, L., M. J. Molemaker, J. Gula, S. Masson, and J. C. McWilliams, 2016a: Control and stabilization of the gulf stream by oceanic current interaction with the atmosphere. *Journal of Physical Oceanography*, **46 (11)**, 3439–3453.

Renault, L., M. J. Molemaker, J. C. McWilliams, A. F. Shchepetkin, F. Lemarié, D. Chelton, S. Illig, and A. Hall, 2016b: Modulation of wind work by oceanic current interaction with the atmosphere. *Journal of Physical Oceanography*, **46 (6)**, 1685–1704.

Rodi, W., 1979: Turbulence models for environmental problems. *Von Karman Inst. for Fluid Dynamics: Prediction Methods for Turbulent Flows*.

Accepted for publication in *Journal of Physical Oceanography*. DOI 10.1175/JPO-D-21-0271.1.

Rodríguez, E., M. Bourassa, D. Chelton, J. T. Farrar, D. Long, D. Perkovic-Martin, and R. Samelson, 2019: The winds and currents mission concept. *Frontiers in Marine Science*, **6**, https://doi.org/10.3389/fmars.2019.00438, URL https://doi.org/10.3389/fmars.2019.00438.

Schmitz, W. J., 2005: Cyclones and westward propagation in the shedding of anticyclonic rings from the loop current. *Circulation in the Gulf of Mexico: Observations and Models*, American Geophysical Union, 241–261, https://doi.org/10.1029/161gm18.

Seo, H., Y.-O. Kwon, T. M. Joyce, and C. C. Ummenhofer, 2017: On the predominant nonlinear response of the extratropical atmosphere to meridional shifts of the gulf stream. *Journal of Climate*, **30 (23)**, 9679–9702, https://doi.org/10.1175/jcli-d-16-0707.1, URL https://doi.org/10.1175/jcli-d-16-0707.1.

Seo, H., A. J. Miller, and J. R. Norris, 2016: Eddy–wind interaction in the california current system: Dynamics and impacts. *Journal of Physical Oceanography*, **46 (2)**, 439–459.

Sheinbaum, J., 2002: Flow structure and transport in the yucatan channel. *Geophysical Research Letters*, **29 (3)**, https://doi.org/10.1029/2001gl013990, URL https://doi.org/10.1029/2001gl013990.

Sheinbaum, J., G. Athié, J. Candela, J. Ochoa, and A. Romero-Arteaga, 2016: Structure and variability of the yucatan and loop currents along the slope and shelf break of the yucatan channel and campeche bank. *Dynamics of Atmospheres and Oceans*, **76**, 217–239, https://doi.org/10.1016/j.dynatmoce.2016.08.001, URL https://doi.org/10.1016/j.dynatmoce.2016.08.001.

Skamarock, W. C., and Coauthors, 2019: A description of the advanced research wrf model version 4. *National Center for Atmospheric Research: Boulder, CO, USA*, 145.

Small, R., and Coauthors, 2008: Air–sea interaction over ocean fronts and eddies. *Dynamics of Atmospheres and Oceans*, **45 (3-4)**, 274–319, https://doi.org/10.1016/j.dynatmoce.2008.01.001, URL https://doi.org/10.1016/j.dynatmoce.2008.01.001.

Sosa-Gutiérrez, R., E. Pallàs-Sanz, J. Jouanno, A. Chaigneau, J. Candela, and M. Tenreiro, 2020: Erosion of the subsurface salinity maximum of the loop current eddies from glider observations and a numerical model. *Journal of Geophysical Research: Oceans*, **125 (7)**, e2019JC015 397.

Accepted for publication in *Journal of Physical Oceanography*. DOI 10.1175/JPO-D-21-0271.1

Sturges, W., and R. Leben, 2000: Frequency of ring separations from the loop current in the gulf of mexico: A revised estimate. *Journal of Physical Oceanography*, **30 (7)**, 1814–1819, https://doi.org/10.1175/1520-0485(2000)030<1814:forsft>2.0.co;2, URL https://doi.org/10.1175/1520-0485(2000)030<1814:forsft>2.0.co;2.

Umlauf, L., and H. Burchard, 2003: A generic length-scale equation for geophysical turbulence models. *Journal of Marine Research*, **61 (2)**, 235–265, https://doi.org/doi:10.1357/002224003322005087, URL https://www.ingentaconnect.com/content/jmr/jmr/2003/00000061/00000002/art00004.

Valcke, S., 2013: The oasis3 coupler: A european climate modelling community software. *Geoscientific Model Development*, **6 (2)**, 373–388.

Vukovich, F. M., and G. A. Maul, 1985: Cyclonic eddies in the eastern gulf of mexico. *Journal of Physical Oceanography*, **15 (1)**, 105–117, https://doi.org/10.1175/1520-0485(1985)015<0105:ceiteg>2.0.co;2, URL https://doi.org/10.1175/1520-0485(1985)015<0105:ceiteg>2.0.co;2.

Wang, M., and C. Hu, 2017: Predicting sargassum blooms in the caribbean sea from MODIS observations. *Geophysical Research Letters*, **44 (7)**, 3265–3273, https://doi.org/10.1002/2017gl072932, URL https://doi.org/10.1002/2017gl072932.

White, H. K., and Coauthors, 2012: Impact of the deepwater horizon oil spill on a deep-water coral community in the gulf of mexico. *Proceedings of the National Academy of Sciences*, **109 (50)**, 20 303–20 308, https://doi.org/10.1073/pnas.1118029109, URL https://doi.org/10.1073/pnas.1118029109.

Yablonsky, R. M., and I. Ginis, 2012: Impact of a warm ocean eddy's circulation on hurricane-induced sea surface cooling with implications for hurricane intensity. *Monthly Weather Review*, **141 (3)**, 997–1021, https://doi.org/10.1175/mwr-d-12-00248.1, URL https://doi.org/10.1175/mwr-d-12-00248.1.

Zalesak, S. T., 1979: Fully multidimensional flux-corrected transport algorithms for fluids. *Journal of Computational Physics*, **31 (3)**, 335–362, https://doi.org/10.1016/0021-9991(79)90051-2, URL https://doi.org/10.1016/0021-9991(79)90051-2.

Accepted for publication in *Journal of Physical Oceanography*. DOI 10.1175/JPO-D-21-0271.1

Zavala-Hidalgo, J., S. Morey, J. O'brien, and L. Zamudio, 2006: On the loop current eddy shedding variability. *Atmósfera*, **19 (1)**, 41–48.

Zavala-Hidalgo, J., S. L. Morey, and J. J. O'Brien, 2003: Cyclonic eddies northeast of the campeche bank from altimetry data. *Journal of Physical Oceanography*, **33 (3)**, 623–629, https://doi.org/10.1175/1520-0485(2003)033<0623:cenotc>2.0.co;2, URL https://doi.org/10.1175/1520-0485(2003)033<0623:cenotc>2.0.co;2.

Zheng, Y., K. Alapaty, J. A. Herwehe, A. D. Del Genio, and D. Niyogi, 2016: Improving high-resolution weather forecasts using the weather research and forecasting (wrf) model with an updated kain–fritsch scheme. *Monthly Weather Review*, **144 (3)**, 833–860.